Frontiers of Information Technology & Electronic Engineering
www.jzus.zju.edu.cn; engineering.cae.cn; www.springerlink.com
ISSN 2095-9184 (print); ISSN 2095-9230 (online)
E-mail: jzus@zju.edu.cn

Target tracking methods based on a signal-to-noise ratio model*

Dai LIU[1,2], Yong-bo ZHAO[†‡1], Zi-qiao YUAN[2], Jie-tao LI[2], Guo-ji CHEN[2]

[1]*National Lab of Radar Signal Processing, Xidian University, Xi'an 710071, China*

[2]*Xi'an Electronic Engineering Research Institute, Xi'an 710100, China*

[†]E-mail: ybzhao@xidian.edu.cn

Received Dec. 4, 2019; Revision accepted Feb. 9, 2020; Crosschecked Nov. 13, 2020

Abstract: In traditional target tracking methods, the angle error and range error are often measured by the empirical value, while observation noise is a constant. In this paper, the angle error and range error are analyzed. They are influenced by the signal-to-noise ratio (SNR). Therefore, a model related to SNR has been established, in which the SNR information is applied for target tracking. Combined with an advanced nonlinear filter method, the extended Kalman filter method based on the SNR model (SNR-EKF) and the unscented Kalman filter method based on the SNR model (SNR-UKF) are proposed. There is little difference between the SNR-EKF and SNR-UKF methods in position precision, but the SNR-EKF method has advantages in computation time and the SNR-UKF method has advantages in velocity precision. Simulation results show that target tracking methods based on the SNR model can greatly improve the tracking performance compared with traditional tracking methods. The target tracking accuracy and convergence speed of the proposed methods have significant improvements.

Key words: Signal-to-noise ratio (SNR) model; Target tracking; Angle error; Range error; Nonlinear filter
https://doi.org/10.1631/FITEE.1900679 **CLC number:** TN953

1 Introduction

With the increasing requirements of weapon systems for tracking and guiding radar, improving the target tracking accuracy has become an important research topic (Tang et al., 2017; Daniyan et al., 2018; Zhang XY et al., 2019; Zhang Y et al., 2019). The current study on target tracking focuses mainly on obtaining more measurement information, which is a requirement of target tracking. The measurement information includes target position, velocity, radial velocity (Ehrman and Lanterman, 2008; Musicki and Song, 2013; Zhou et al., 2014), target pose (Liu D et al., 2019), high-resolution range profile (HRRP) (Hong et al., 2004; Ruan and Hong, 2006; Du et al., 2007), radar cross section (RCS) (Ehrman and Mahapatra, 2009), and target amplitude (Brekke et al., 2010; Mertens et al., 2016). These measurements have been applied to the target measurement equation to improve the target tracking performance. The radial velocity has been introduced to the measurement equation of the Kalman filter to improve the target tracking accuracy (Ehrman and Lanterman, 2008; Musicki and Song, 2013; Zhou et al., 2014). Two target tracking methods aided by the pose of the target have been proposed to improve the prediction accuracy (Liu D et al., 2019). A feature-aided tracking method has been proposed, which uses high-resolution range (HRR) features and the technique of mixture density estimation (Ruan and Hong, 2006). The HRR measurement has been used for ground moving-target tracking and identification (Hong et al., 2004). Complex HRRP has been exploited to obtain better recognition results (Du et al., 2007). RCS-assisted tracking has been used and it is effective when targets are closely spaced (Ehrman and Mahapatra, 2009). RCS information has been exploited to

‡ Corresponding author

* Project supported by the National Natural Science Foundation of China (No. 61671357)

ORCID: Dai LIU, https://orcid.org/0000-0001-7794-6468; Yong-bo ZHAO, https://orcid.org/0000-0002-6453-0786

improve radar performance in some situations (Mertens et al., 2016). Amplitude information has been used to the probabilistic data association filter to improve the radar performance (Brekke et al., 2010). Brekke et al. (2011) proposed that the probabilistic data association filter with amplitude information can safely operate in the presence of abundant clutter.

With the rapid development of radar technology, it is possible to obtain the signal-to-noise ratio (SNR) information of the target with high precision (Das and Rao, 2012; Villano, 2014). Accurate SNR and noise variance estimation has been addressed in multiple-input multiple-output (MIMO) systems (Das and Rao, 2012). The estimation of the noise variance and SNR of the cross-polarized channels has been discussed in synthetic aperture radar (SAR) data (Villano, 2014). The SNR information is applied to radar target tracking in this study.

Compared with traditional target tracking methods, SNR information is extended to the radar target tracking method in this study. The relationships among the range error, angle error, and SNR are analyzed. The SNR model is established, and the measurement noise matrix in the filter method is modified. In traditional target tracking methods, the angle error and range error are fixed at constant values. In contrast, the angle error and range error vary with SNR in the proposed methods. Combined with advanced nonlinear filter methods, including the extended Kalman filter (EKF) method (Barczyk et al., 2015; Rashedi et al., 2018; Xi et al., 2018) and the unscented Kalman filter (UKF) method (Liu CY et al., 2011; Gokce and Kuzuoglu, 2015; Menegaz et al., 2019), the EKF method based on the SNR model (SNR-EKF) and the UKF method based on the SNR model (SNR-UKF) are proposed. Simulation results show that the proposed methods have higher tracking accuracy and higher convergence speed than traditional target tracking methods.

2 Mathematical model

Assume that the target state equation is

$$\boldsymbol{X}_k = \boldsymbol{F}_{k|k-1}\boldsymbol{X}_{k-1} + \boldsymbol{V}_{k-1}, \tag{1}$$

where $\boldsymbol{X}_k=[x_k, \dot{x}_k, y_k, \dot{y}_k, z_k, \dot{z}_k]^{\mathrm{T}}$ represents the state vector at time k, and (x_k, y_k, z_k) and $(\dot{x}_k, \dot{y}_k, \dot{z}_k)$ are the position and velocity of the target at time k, respectively. $\boldsymbol{F}_{k|k-1}$ represents the target state transitional matrix:

$$\boldsymbol{F}_{k|k-1}=\begin{bmatrix} 1 & T & 0 & 0 & 0 & 0 \\ 0 & 1 & 0 & 0 & 0 & 0 \\ 0 & 0 & 1 & T & 0 & 0 \\ 0 & 0 & 0 & 1 & 0 & 0 \\ 0 & 0 & 0 & 0 & 1 & T \\ 0 & 0 & 0 & 0 & 0 & 1 \end{bmatrix},$$

where T refers to the sampling interval. $\boldsymbol{V}_{k-1}$ represents the process noise with state noise intensity σ_w^2 and covariance $\boldsymbol{Q}$:

$$\boldsymbol{Q}=\sigma_w^2\begin{bmatrix} \frac{T^3}{3} & \frac{T^2}{2} & 0 & 0 & 0 & 0 \\ \frac{T^2}{2} & T & 0 & 0 & 0 & 0 \\ 0 & 0 & \frac{T^3}{3} & \frac{T^2}{2} & 0 & 0 \\ 0 & 0 & \frac{T^2}{2} & T & 0 & 0 \\ 0 & 0 & 0 & 0 & \frac{T^3}{3} & \frac{T^2}{2} \\ 0 & 0 & 0 & 0 & \frac{T^2}{2} & T \end{bmatrix}.$$

Suppose that the target's measurement equation is

$$\boldsymbol{Z}_k = h(\boldsymbol{X}_k) + \boldsymbol{W}_k, \tag{2}$$

where $\boldsymbol{Z}_k$ represents the measurement at time k, $h(\cdot)$ the measurement function, and $\boldsymbol{W}_k$ the measurement noise at time k.

The variance of the measurement noise is given as

$$E[\boldsymbol{W}_k\boldsymbol{W}_j^{\mathrm{T}}] = \boldsymbol{R}_k\delta_{kj},$$

where

$$\delta_{kj}=\begin{cases} 1, & k=j, \\ 0, & k\neq j. \end{cases}$$

If $\boldsymbol{Z}_k=[\rho_k, \theta_k, \varphi_k]^{\mathrm{T}}$, then

$$h(\boldsymbol{X}_k)=\begin{bmatrix}\sqrt{x_k^2+y_k^2+z_k^2}\\ \operatorname{atan}(y_k/x_k)\\ \operatorname{atan}\left(z_k\Big/\sqrt{x_k^2+y_k^2}\right)\end{bmatrix},$$

$$\boldsymbol{R}_k=\begin{bmatrix}\sigma_{\rho_k}^2 & 0 & 0\\ 0 & \sigma_{\theta_k}^2 & 0\\ 0 & 0 & \sigma_{\varphi_k}^2\end{bmatrix}.$$

If $\boldsymbol{Z}_k=[x_k, y_k, z_k]^{\mathrm{T}}$, then

$$h(\boldsymbol{X}_k)=(x_k, y_k, z_k)^{\mathrm{T}},$$

$$\boldsymbol{R}_k=\boldsymbol{A}\begin{bmatrix}\sigma_{\rho_k}^2 & 0 & 0\\ 0 & \sigma_{\theta_k}^2 & 0\\ 0 & 0 & \sigma_{\varphi_k}^2\end{bmatrix}\boldsymbol{A}^{\mathrm{T}},$$

$$\boldsymbol{A}=\begin{bmatrix}\cos\theta_k\cos\varphi_k & -\rho_k\sin\theta_k\cos\varphi_k & -\rho_k\cos\theta_k\sin\varphi_k\\ \sin\theta_k\cos\varphi_k & \rho_k\cos\theta_k\cos\varphi_k & -\rho_k\sin\theta_k\sin\varphi_k\\ \sin\varphi_k & 0 & \rho_k\cos\varphi_k\end{bmatrix},$$

where ρ_k, θ_k, and φ_k represent the range, azimuth, and elevation of the target in the polar coordinate system at time k, respectively, (x_k, y_k, z_k) represents the position of the target in the Cartesian coordinate system at time k, $\sigma_{\rho_k}^2$ represents the variance of the range measurement error at time k, $\sigma_{\theta_k}^2$ represents the variance of the azimuth measurement error at time k, and $\sigma_{\varphi_k}^2$ represents the variance of the elevation measurement error at time k. In this study, we adopt $\boldsymbol{Z}_k=[\rho_k, \theta_k, \varphi_k]$ for the convenience of analysis. In traditional target tracking methods, $\sigma_{\rho_k}^2$, $\sigma_{\theta_k}^2$, and $\sigma_{\varphi_k}^2$ are empirical constants.

3 Target tracking methods based on the SNR model

3.1 SNR analysis

The expression between the minimum detection SNR and the range can be described as (Skolnik, 1962)

$$\mathrm{SNR}_{\min}=\frac{P_{\mathrm{t}}G_{\mathrm{t}}G_{\mathrm{r}}\lambda^2\sigma}{(4\pi)^3k_1T_0BFLR^4}, \tag{3}$$

where $\mathrm{SNR}_{\min}$ denotes the minimum detection SNR, R the target range, P_{t} the average power of the transmitter, G_{t} the transmit gain of the antenna, G_{r} the receive gain of the antenna, λ the wavelength, σ the RCS of the target, B the receiver bandwidth, F the receiver noise coefficient, L the radar loss, k_1 the Boltzmann constant, and T_0 the standard room temperature.

Suppose σ=0.1, 1, or 10 m^2, P_{t}=1500 W, λ=0.0536 m, G_{t}=G_{r}=45, B=5×10^6 Hz, F=3, L=6. As shown in Fig. 1, the SNR decreases with the increase of the target range. At the same range, the larger the RCS of the target, the larger the SNR of the target.

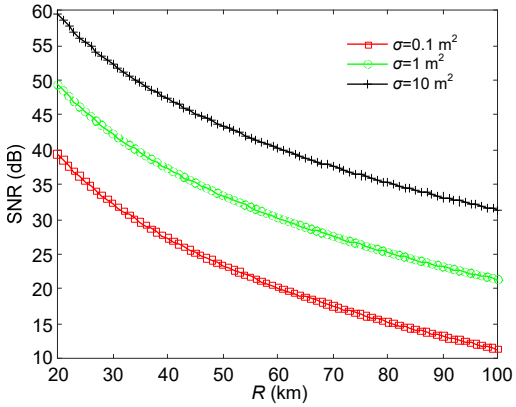

Fig. 1 Relationship between SNR and the target range at different σ's

3.2 Angle error analysis

The angle error caused by the thermal noise of the receiver is described as

$$\sigma_{\phi 1}=\frac{\mathrm{BW}}{K_{\mathrm{m}}\sqrt{2\mathrm{SNR}}}, \tag{4}$$

where BW denotes the 3-dB beam width and K_{m} denotes the single pulse angle slope.

As shown in Fig. 2, the angle error varies with SNR when K_{m}=1.5 and BW=1°, 2°, or 3°. It can be seen that the angle error caused by the thermal noise of the receiver depends on the antenna beam width and SNR. Under the same antenna beam width, the larger the SNR of the target, the smaller the angle error caused by the thermal noise of the receiver. Under the same SNR condition, the narrower the

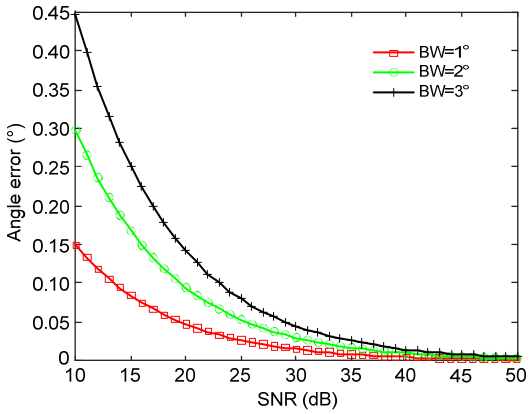

Fig. 2 Relationship between the angle error and SNR at different BW's when K_m=1.5

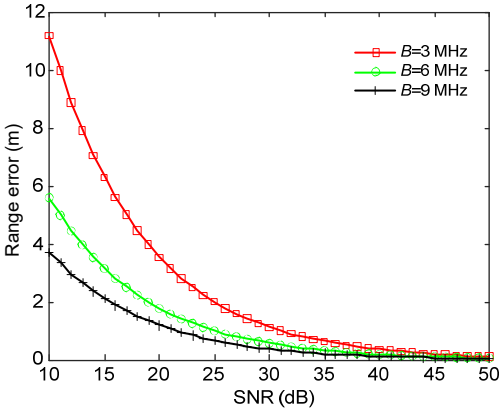

Fig. 3 Relationship between the range error and SNR at different B's

antenna beam width, the smaller the angle error caused by the thermal noise of the receiver.

In fact, the angle error of a radar is not only related to the thermal noise of the receiver, but also affected by factors such as angular glint, quantization error of angle coding, sampling quantization error, amplitude-phase imbalance, and atmospheric refraction. However, the thermal noise of the receiver is the main factor resulting in an angle error. Assume that the angle error caused by other factors except the thermal noise of the receiver is $\sigma_{\phi 2}$.

Because $\sigma_{\phi 1}$ and $\sigma_{\phi 2}$ are independent, there exists

$$\sigma_{\phi}^2=\sigma_{\phi 1}^2+\sigma_{\phi 2}^2. \tag{5}$$

3.3 Range error analysis

The range error caused by the thermal noise of the receiver is described as follows:

$$\sigma_{\rho 1}=\frac{c}{2B_s\sqrt{2\mathrm{SNR}}}, \tag{6}$$

where B_s is the signal bandwidth and c the propagation speed of the electromagnetic wave.

As shown in Fig. 3, the range error varies with SNR when B=3, 6, or 9 MHz. It can be seen that the range error caused by the thermal noise of the receiver depends on the signal bandwidth and SNR. With the same signal bandwidth, the larger the SNR of the target, the smaller the range error caused by the thermal noise of the receiver. Under the same SNR condition, the larger the signal bandwidth, the smaller the range error caused by the thermal noise of the receiver.

In fact, the range error of a radar is not only related to the thermal noise of the receiver, but also affected by factors such as angular glint, range quantization error, multipath, transmitted pulse jitter, range Doppler coupling, and atmospheric refraction. Assume that the range error caused by factors other than the thermal noise of the receiver is $\sigma_{\rho 2}$.

Because $\sigma_{\rho 1}$ and $\sigma_{\rho 2}$ are independent, there exists

$$\sigma_{\rho}^2=\sigma_{\rho 1}^2+\sigma_{\rho 2}^2. \tag{7}$$

3.4 Implementation of target tracking methods

3.4.1 Selection of measurement noise covariance

The minimum SNR is calculated according to the detection probability and false alarm probability determined by a radar (Alberhseim, 1981; Tufts and Cann, 1983):

$$\mathrm{SNR}_{\min}=A+0.12AB+1.7B, \tag{8}$$

where A=ln(0.62/P_{fa}) and B=ln(P_{d}/(1−P_{d})). P_{fa} denotes the false alarm probability and P_{d} the detection probability.

Assume that the target SNR at time k is SNR_k. Then we have $\mathrm{SNR}_k \geq \mathrm{SNR}_{\min}$. According to Eqs. (4)–(7), the measurement noise covariance at time k in the polar coordinate system can be obtained as follows:

$$
\begin{aligned}
\boldsymbol{R}_k &= \begin{bmatrix} \sigma_{\rho_k}^2 & 0 & 0 \\ 0 & \sigma_{\theta_k}^2 & 0 \\ 0 & 0 & \sigma_{\varphi_k}^2 \end{bmatrix} \\
&= \begin{bmatrix} \sigma_{\rho 1_k}^2+\sigma_{\rho 2_k}^2 & 0 & 0 \\ 0 & \sigma_{\theta 1_k}^2+\sigma_{\theta 2_k}^2 & 0 \\ 0 & 0 & \sigma_{\varphi 1_k}^2+\sigma_{\varphi 2_k}^2 \end{bmatrix} \\
&= \begin{bmatrix} \sigma_{\rho 1_k}^2 & 0 & 0 \\ 0 & \sigma_{\theta 1_k}^2 & 0 \\ 0 & 0 & \sigma_{\varphi 1_k}^2 \end{bmatrix} + \begin{bmatrix} \sigma_{\rho 2_k}^2 & 0 & 0 \\ 0 & \sigma_{\theta 2_k}^2 & 0 \\ 0 & 0 & \sigma_{\varphi 2_k}^2 \end{bmatrix} \\
&= \begin{bmatrix} \dfrac{c^2}{8B_{\mathrm{s}}^2\mathrm{SNR}_k} & 0 & 0 \\ 0 & \dfrac{\theta_{\mathrm{H}}^2}{2K_{\mathrm{m}}^2\mathrm{SNR}_k} & 0 \\ 0 & 0 & \dfrac{\varphi_{\mathrm{H}}^2}{2K_{\mathrm{m}}^2\mathrm{SNR}_k} \end{bmatrix} \\
&\quad + \begin{bmatrix} \sigma_{\rho 2_k}^2 & 0 & 0 \\ 0 & \sigma_{\theta 2_k}^2 & 0 \\ 0 & 0 & \sigma_{\varphi 2_k}^2 \end{bmatrix} \\
&= \boldsymbol{R}_{k1} + \boldsymbol{R}_{k2},
\end{aligned} \tag{9}
$$

where θ_{H} denotes the azimuth 3-dB beam width, and φ_{H} denotes the elevation 3-dB beam width.

$$
\boldsymbol{R}_{k1} = \begin{bmatrix} \dfrac{c^2}{8B_{\mathrm{s}}^2\mathrm{SNR}_k} & 0 & 0 \\ 0 & \dfrac{\theta_{\mathrm{H}}^2}{2K_{\mathrm{m}}^2\mathrm{SNR}_k} & 0 \\ 0 & 0 & \dfrac{\varphi_{\mathrm{H}}^2}{2K_{\mathrm{m}}^2\mathrm{SNR}_k} \end{bmatrix} \tag{10}
$$

denotes the measurement noise covariance caused by the thermal noise of the receiver, and $\boldsymbol{R}_{k2}$ denotes the measurement noise covariance caused by the other factors.

3.4.2 Extended Kalman filter method based on the SNR model

The SNR-EKF method applies the target SNR information to the EKF method. Supposing that the target state and covariance matrix are respectively $\hat{\boldsymbol{X}}_{k-1|k-1}$ and $\boldsymbol{P}_{k-1|k-1}$ at time $k-1$, $\boldsymbol{z}_k=[\rho_k, \theta_k, \varphi_k]^{\mathrm{T}}$, SNR_k is the target SNR at time k, and $\boldsymbol{R}_{k2}$ is the measurement noise covariance caused by factors other than the thermal noise of the receiver at time k, the detailed steps of the SNR-EKF method are as follows:

Step 1: judge whether SNR_k satisfies the condition $\mathrm{SNR}_k \geq \mathrm{SNR}_{\min}$. If it does, turn to step 2.

Step 2: calculate $\boldsymbol{R}_{k1}$ according to Eq. (10), and then substitute it into Eq. (9) to obtain $\boldsymbol{R}_k$.

Step 3: predict the state:

$$
\hat{\boldsymbol{X}}_{k|k-1} = \boldsymbol{F}\hat{\boldsymbol{X}}_{k-1|k-1}, \tag{11}
$$

$$
\boldsymbol{P}_{k|k-1} = \boldsymbol{F}\boldsymbol{P}_{k-1|k-1}\boldsymbol{F}^{\mathrm{T}} + \boldsymbol{Q}_{k-1}. \tag{12}
$$

Step 4: update the state:

$$
\boldsymbol{K}_k = \boldsymbol{P}_{k|k-1}\boldsymbol{H}_k\boldsymbol{S}_k^{-1}, \tag{13}
$$

$$
\hat{\boldsymbol{X}}_{k|k} = \hat{\boldsymbol{X}}_{k|k-1} + \boldsymbol{K}_k\left(\boldsymbol{z}_k - h\left(\hat{\boldsymbol{X}}_{k|k-1}\right)\right), \tag{14}
$$

$$
\boldsymbol{P}_{k|k} = [\boldsymbol{I} - \boldsymbol{K}_k\boldsymbol{H}_k]\boldsymbol{P}_{k|k-1}[\boldsymbol{I} - \boldsymbol{K}_k\boldsymbol{H}_k]^{\mathrm{T}} - \boldsymbol{K}_k\boldsymbol{R}_k\boldsymbol{K}_k^{\mathrm{T}}, \tag{15}
$$

where

$$
\begin{cases} \boldsymbol{H}_k = \left(\Delta_{x_k}\left(h(\boldsymbol{X}_k)\right)^{\mathrm{T}}\right)^{\mathrm{T}}, \\ \boldsymbol{S}_k = \boldsymbol{H}_k\boldsymbol{P}_{k|k-1}\boldsymbol{H}_k^{\mathrm{T}} + \boldsymbol{R}_k. \end{cases}
$$

3.4.3 Unscented Kalman filter method based on the SNR model

The SNR-UKF method applies the target SNR information to the UKF method. The assumption of the SNR-UKF method is the same as that of the SNR-EKF method. The detailed steps of the SNR-UKF method are as follows:

Step 1: judge whether SNR_k satisfies the condition $\mathrm{SNR}_k \geq \mathrm{SNR}_{\min}$. If it does, turn to step 2.

Step 2: calculate $\boldsymbol{R}_{k1}$ according to Eq. (10), and then substitute it into Eq. (9) to obtain $\boldsymbol{R}_k$.

Step 3: update the time:

$$
\begin{cases} \boldsymbol{\chi}_{k-1|k-1}^0 = \hat{\boldsymbol{X}}_{k-1|k-1}, \\ \boldsymbol{\chi}_{k-1|k-1}^i = \hat{\boldsymbol{X}}_{k-1|k-1} + \sqrt{(n+\lambda)\boldsymbol{P}_{k-1|k-1}}, \\ \qquad\qquad i = 1,2,...,n, \\ \boldsymbol{\chi}_{k-1|k-1}^i = \hat{\boldsymbol{X}}_{k-1|k-1} - \sqrt{(n+\lambda)\boldsymbol{P}_{k-1|k-1}}, \\ \qquad\qquad i = n+1,n+2,...,2n, \end{cases} \tag{16}
$$

$$\begin{cases} \omega_0^m = \dfrac{\kappa}{n+\kappa}, \\ \omega_0^c = \dfrac{\kappa}{n+\kappa} + 1 - \alpha^2 + \gamma, \\ \omega_i^m = \omega_i^c = \dfrac{\kappa}{2(n+\kappa)}, i = 1,2,...,2n, \end{cases} \tag{17}$$

$$\boldsymbol{\chi}_{k|k-1}^i = \boldsymbol{F}\boldsymbol{\chi}_{k-1|k-1}^i, \tag{18}$$

$$\hat{\boldsymbol{X}}_{k|k-1} = \sum_{i=0}^{2n} \omega_i^m \boldsymbol{\chi}_{k|k-1}^i, \tag{19}$$

$$\boldsymbol{P}_{k|k-1} = \sum_{i=0}^{2n} \omega_i^c (\boldsymbol{\chi}_{k|k-1}^i - \hat{\boldsymbol{X}}_{k|k-1})(\boldsymbol{\chi}_{k|k-1}^i - \hat{\boldsymbol{X}}_{k|k-1})^{\mathrm{T}} + \boldsymbol{Q}_{k-1}. \tag{20}$$

Step 4: update the measurement:

$$\boldsymbol{\xi}_{k|k-1}^i = h(\boldsymbol{\chi}_{k|k-1}^i), \tag{21}$$

$$\hat{\boldsymbol{z}}_{k|k-1} = \sum_{i=0}^{2n} \omega_i^m \boldsymbol{\xi}_{k|k-1}^i, \tag{22}$$

$$\boldsymbol{P}_{z_k} = \sum_{i=0}^{2n} \omega_i^c (\boldsymbol{\xi}_{k|k-1}^i - \hat{\boldsymbol{z}}_{k|k-1})(\boldsymbol{\xi}_{k|k-1}^i - \hat{\boldsymbol{z}}_{k|k-1})^{\mathrm{T}} + \boldsymbol{R}_k, \tag{23}$$

$$\boldsymbol{P}_{x_k z_k} = \sum_{i=0}^{2n} \omega_i^c (\boldsymbol{\chi}_{k|k-1}^i - \hat{\boldsymbol{X}}_{k|k-1})(\boldsymbol{\xi}_{k|k-1}^i - \hat{\boldsymbol{z}}_{k|k-1})^{\mathrm{T}}, \tag{24}$$

where ω_i^c is the weight to obtain the estimated mean of $\boldsymbol{\chi}_{k-1|k-1}^i$, ω_i^m is the weight to obtain the estimated covariance matrix of $\boldsymbol{\chi}_{k-1|k-1}^i$, $\hat{\boldsymbol{X}}_{k|k-1}$ is the predicted target state at time k, and $\boldsymbol{P}_{k|k-1}$ is the predicted covariance matrix at time k.

Step 5: update the filter:

$$\boldsymbol{K}_k = \boldsymbol{P}_{z_k} \boldsymbol{P}_{x_k z_k}^{-1}, \tag{25}$$

$$\hat{\boldsymbol{X}}_{k|k} = \hat{\boldsymbol{X}}_{k|k-1} + \boldsymbol{K}_k(\boldsymbol{z}_k - \hat{\boldsymbol{z}}_{k|k-1}), \tag{26}$$

$$\boldsymbol{P}_{k|k} = \boldsymbol{P}_{k|k-1} - \boldsymbol{K}_k \boldsymbol{P}_{z_k} \boldsymbol{K}_k^{\mathrm{T}}, \tag{27}$$

where $\boldsymbol{K}_k$ is the Kalman gain, $\hat{\boldsymbol{X}}_{k|k}$ is the target state at time k, and $\boldsymbol{P}_{k|k}$ is the covariance matrix at time k.

4 Simulations and analysis

To verify the effectiveness of the proposed methods, simulations have been conducted as follows: the target keeps 1000 m away from the initial position (10 000, 10 000, 1000) m, and moves in a uniform straight line at a speed of (100, −120) m/s. The target trajectory is shown in Fig. 4. The radar system parameters are as follows: P_t=5000 W, λ=0.056 m, G_t=G_r=45, B=5×10^6 Hz, F=3, L=6, σ=0.1 m^2, P_d=50%, P_{fa}=10^{-6}, $\sigma_{\rho 2}$=15 m, $\sigma_{\phi 2}$=0.0286°. Bringing P_d and P_{fa} into Eq. (8), there exists SNR_{min}=13.3 dB. Two hundred Monte-Carlo simulations have been carried out with the observation data interval of 1 s and duration of 100 s. The process noise is the white noise with a mean value of 0 and state noise intensity of 1.

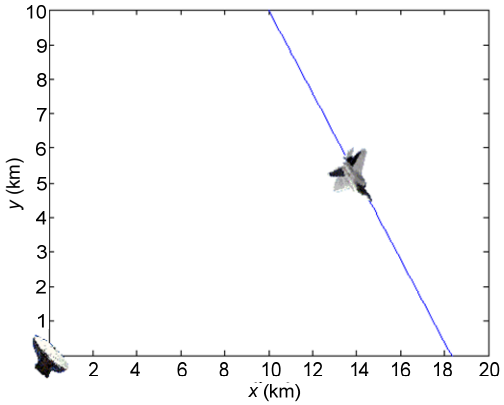

Fig. 4 Trajectory of the target

Three scenarios are simulated here:

Scenario 1 The range error remains unchanged at 30 m, and the angle error varies with SNR.

This scenario is designed to verify the effect of SNR on the angle error and target tracking performance.

Scenario 2 The angle error remains unchanged at 0.0432°, and the range error varies with SNR.

This scenario is designed to verify the effect of SNR on the range error and target tracking performance.

Scenario 3 The angle error and range error vary with SNR.

This scenario is designed to verify the effect of SNR on the range error, angle error, and target tracking performance. The range error of the EKF and UKF methods is 30 m, and the angle error is 0.0432°.

The SNR-EKF method, SNR-UKF method, traditional EKF method, and traditional UKF method are compared in the following four aspects: position precision, velocity precision, convergence speed, and computation time.

The root mean square errors (RMSEs) of the target position and target velocity are as follows:

$$\mathrm{RMSE}_{pk}=\sqrt{\frac{1}{M}\sum_{i=1}^{M}[(x_k-x_k^i)^2+(y_k-y_k^i)^2]}, \quad (28)$$

$$\mathrm{RMSE}_{vk}=\sqrt{\frac{1}{M}\sum_{i=1}^{M}[(\dot{x}_k-\dot{x}_k^i)^2+(\dot{y}_k-\dot{y}_k^i)^2]}, \quad (29)$$

where M is the number of simulations, (x_k^i, y_k^i) is the estimated target position, and $(\dot{x}_k^i, \dot{y}_k^i)$ is the estimated target velocity in the i^{th} simulation.

According to radar parameters and the target route, the SNR variation can be obtained using Eq. (3). As shown in Fig. 5, with the increase of the target range, the target SNR decreases from 40.52 to 34.53 dB. The azimuth error is generated by Eq. (4) and the range error is generated by Eq. (6) in real time. From the angle error curve in Fig. 6, it can be seen that with the increase of the target range, the angle error increases from 0.0384° to 0.0481°. From the range error curve in Fig. 7, it can be seen that with the increase of the target range, the range error increases from 25 to 34.9 m.

The simulation results for Scenario 1 are shown in Figs. 8–10.

From Fig. 8, we can see that the RMSEs of the target position of the traditional EKF and UKF methods are both 38.7 m, while the RMSEs of the target position of the SNR-UKF method and the SNR-EKF method are both 29.7 m; the position accuracy is improved by 9 m. Compared with the traditional EKF and UKF methods, the SNR-UKF method and the SNR-EKF method converge faster and have a

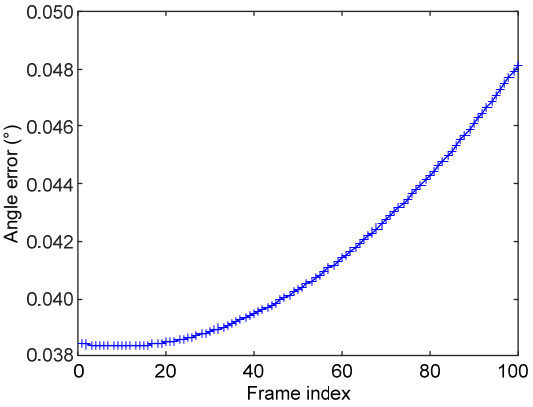

Fig. 6 Angle error curve

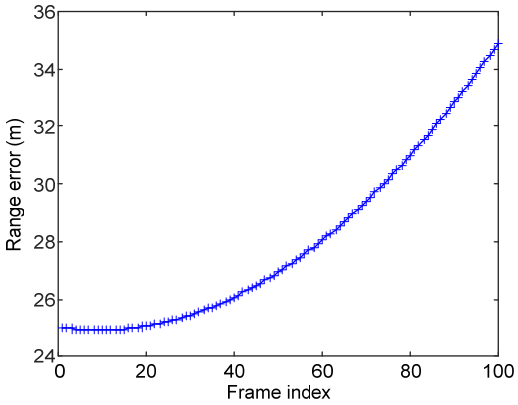

Fig. 7 Range error curve

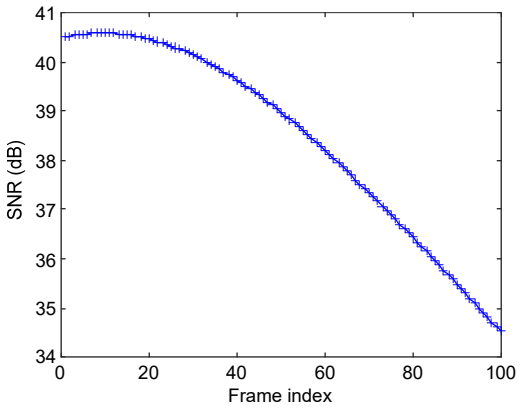

Fig. 5 SNR variation curve

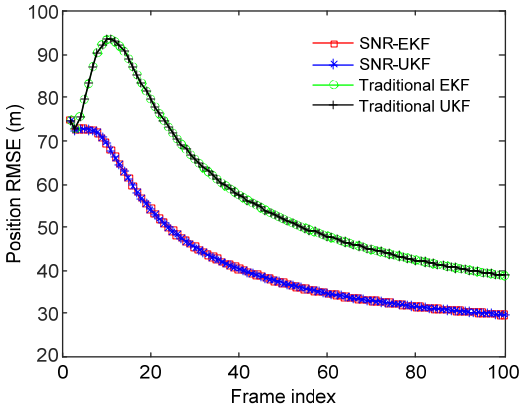

Fig. 8 RMSEs of the target position for scenario 1

higher position accuracy. The performance of the SNR-UKF method is similar to that of the SNR-EKF method.

From Fig. 9, it can be seen that the RMSE of the target velocity of the SNR-UKF method is 22.6 m/s, that of the traditional UKF method is 23.1 m/s, that of the SNR-EKF method is 31.98 m/s, and that of the traditional EKF method is 32.49 m/s. The velocity accuracy of the SNR-UKF method is 9.89 m/s higher than that of the traditional EKF method. The RMSE of the target velocity of the SNR-UKF method is the smallest and its velocity accuracy is the highest.

Fig. 10 shows that the computation time of the SNR-EKF method and the traditional EKF method is maintained at 64 μs, while that of the SNR-UKF method and the traditional UKF method is maintained at 153 μs. The SNR-EKF method and the traditional EKF method are the best on computation time. Compared with the SNR-UKF method, the SNR-EKF method is better on computation time.

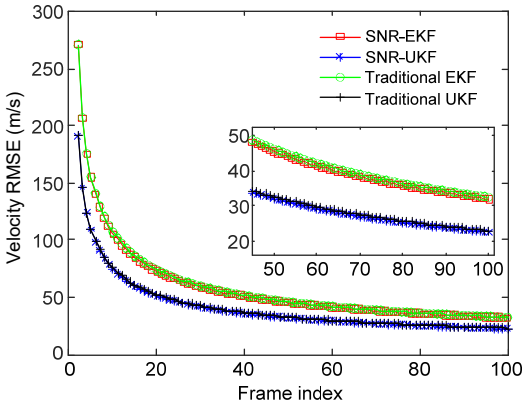

Fig. 9 RMSEs of the target velocity for scenario 1

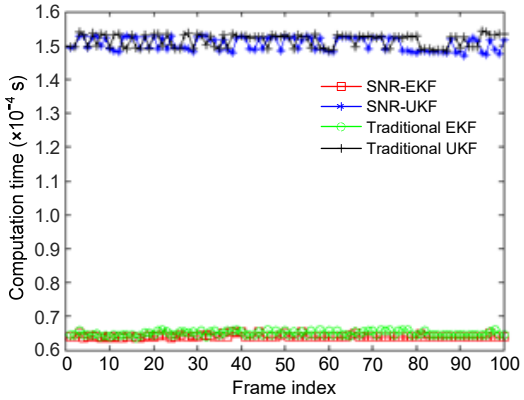

Fig. 10 Computation time of the four methods for scenario 1

From Figs. 8 and 9, it can be seen that the EKF method and the UKF method are sensitive to the value of the angle error. The angle error matching with the target SNR is conducive to improving performance.

The simulation results for Scenario 2 are shown in Figs. 11–13.

From Fig. 11, we can see that the RMSEs of the target position of the traditional EKF and UKF methods are both 35.0 m, while those of the SNR-UKF and SNR-EKF methods are both 27.0 m; the position accuracy is improved by 8.0 m. Compared with the traditional EKF and UKF methods, the SNR-UKF and SNR-EKF methods converge faster and have a higher position accuracy. The performance of the SNR-UKF method is similar to that of the SNR-EKF method.

From Fig. 12, it can be seen that the RMSE of the target velocity of the SNR-UKF method is 22.74 m/s, that of the traditional UKF method is 22.86 m/s, that of the SNR-EKF method is 31.88 m/s, and that of the

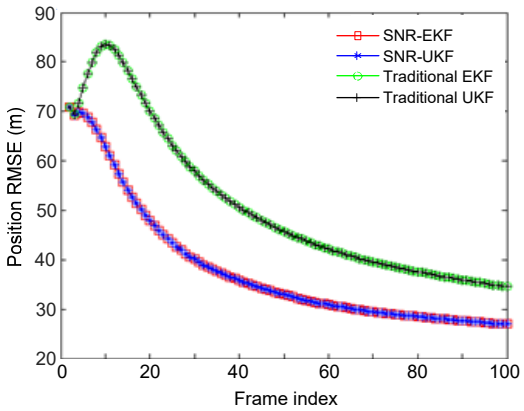

Fig. 11 RMSEs of the target position for scenario 2

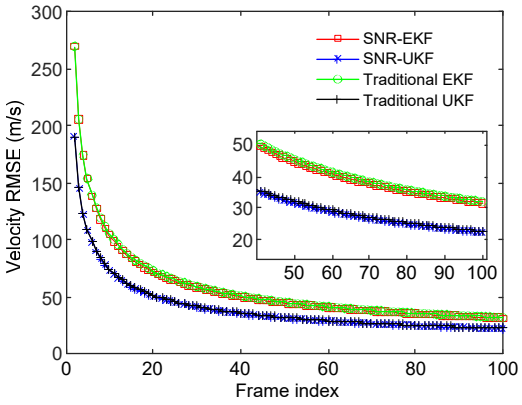

Fig. 12 RMSEs of the target velocity for scenario 2

traditional EKF method is 32.32 m/s. The velocity accuracy of the SNR-UKF method is 9.58 m/s higher than that of the traditional EKF method. The RMSE of the target velocity of the SNR-UKF method is the smallest and its velocity accuracy is the highest.

Fig. 13 shows that the computation time of the SNR-EKF method and the traditional EKF method is maintained at 63 μs, while that of the SNR-UKF method and the traditional UKF method is maintained at 152 μs. The SNR-EKF method and the traditional EKF method are the best on computation time. Compared with the SNR-UKF method, the SNR-EKF method is better on computation time.

From Figs. 11 and 12, it can be seen that the EKF method and the UKF method are sensitive to the value of the range error. The range error matching with the target SNR is conducive to improving performance.

The simulation results for Scenario 3 are shown in Figs. 14–16.

From Fig. 14, we can see that the RMSEs of the target position of the traditional EKF method and the UKF method are both 34.4 m, while those of the SNR-UKF and SNR-EKF methods are both 21.4 m, which means that the position accuracy is improved by 13 m. Compared with the traditional EKF and UKF methods, the SNR-UKF and SNR-EKF methods converge faster and have a higher position accuracy. The performance of the SNR-UKF method is similar to that of the SNR-EKF method.

From Fig. 15, it can be seen that the RMSE of the target velocity of the SNR-UKF method is 22.29 m/s, that of the traditional UKF method is 22.74 m/s, that of the SNR-EKF method is 31.53 m/s, and that of the traditional EKF method is 32.16 m/s. The velocity accuracy of the SNR-UKF method is 9.87 m/s higher than that of the traditional EKF method. The RMSE of the target velocity of the SNR-UKF method is the smallest and its velocity accuracy is the highest.

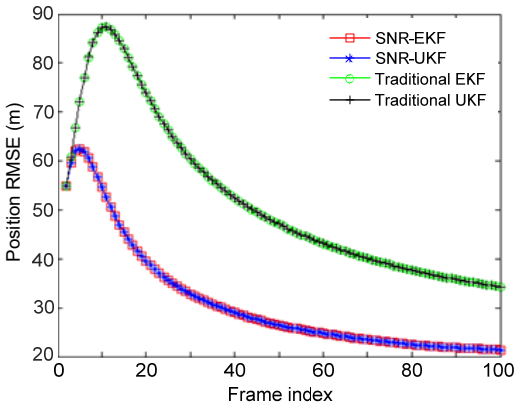

Fig. 14 RMSEs of the target position for scenario 3

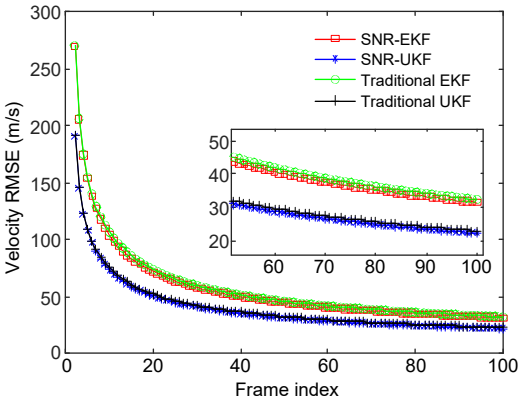

Fig. 15 RMSEs of the target velocity for scenario 3

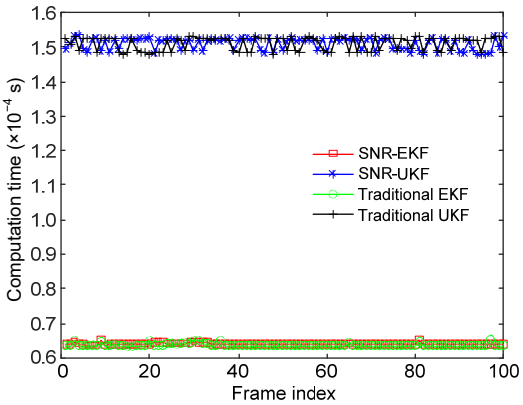

Fig. 13 Computation time of the four methods for scenario 2

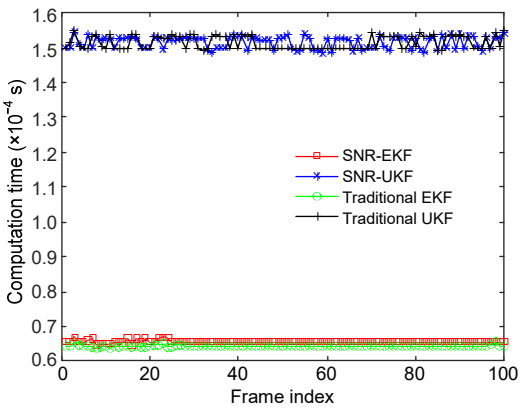

Fig. 16 Computation time of the four methods for scenario 3

Fig. 16 shows that the computation time of the SNR-EKF method and the traditional EKF method is maintained at 65 μs, while that of the SNR-UKF method and the traditional UKF method is maintained at 153 μs. The SNR-EKF method and the traditional EKF method are the best on computation time. Compared with the SNR-UKF method, the SNR-EKF method is better on computation time.

From Figs. 14 and 15, it can be seen that the EKF method and the UKF method are sensitive to the value of the range error and the angle error. The range error and the angle error matching with the target SNR are conducive to improving performance.

5 Conclusions

In this paper, the SNR-EKF method and the SNR-UKF method have been proposed based on the SNR model. Through simulation analysis, the conclusions are as follows:

1. Compared with the traditional EKF method and the UKF method, the SNR-EKF method and the SNR-UKF method have superior performance (higher prediction accuracy and higher convergence speed) and little influence on computation time.

2. Compared with the SNR-EKF method, the SNR-UKF method has higher velocity precision, but longer computation time, and their position precision is almost the same.

Contributors

Dai LIU designed the research. Dai LIU and Yong-bo ZHAO processed the data. Dai LIU drafted the manuscript. Zi-qiao YUAN, Jie-tao LI, and Guo-ji CHEN helped organize the manuscript. Dai LIU and Yong-bo ZHAO revised and finalized the paper.

Compliance with ethics guidelines

Dai LIU, Yong-bo ZHAO, Zi-qiao YUAN, Jie-tao LI, and Guo-ji CHEN declare that they have no conflict of interest.

References

Alberhseim WJ, 1981. A closed-form approximation to Robertson's detection characteristics. *Proc IEEE*, 69(7):839. https://doi.org/10.1109/PROC.1981.12082

Barczyk M, Bonnabel S, Deschaud JE, et al., 2015. Invariant EKF design for scan matching-aided localization. *IEEE Trans Contr Syst Technol*, 23(6):2440-2448. https://doi.org/10.1109/TCST.2015.2413933

Brekke E, Hallingstad O, Glattetre J, 2010. Tracking small targets in heavy-tailed clutter using amplitude information. *IEEE J Ocean Eng*, 35(2):314-329. https://doi.org/10.1109/JOE.2010.2044670

Brekke E, Hallingstad O, Glattetre J, 2011. The modified Riccati equation for amplitude-aided target tracking in heavy-tailed clutter. *IEEE Trans Aerosp Electron Syst*, 47(4):2874-2886. https://doi.org/10.1109/TAES.2011.6034670

Daniyan A, Lambotharan S, Deligiannis A, et al., 2018. Bayesian multiple extended target tracking using labeled random finite sets and splines. *IEEE Trans Signal Process*, 66(22):6076-6091. https://doi.org/10.1109/TSP.2018.2873537

Das A, Rao BD, 2012. SNR and noise variance estimation for MIMO systems. *IEEE Trans Signal Process*, 60(8):3929-3941. https://doi.org/10.1109/TSP.2012.2194707

Du L, Liu H, Bao Z, et al., 2007. Radar automatic target recognition using complex high-resolution range profiles. *IET Radar Sonar Nav*, 1(1):18-26. https://doi.org/10.1049/iet-rsn:20050119

Ehrman LM, Lanterman AD, 2008. Extended Kalman filter for estimating aircraft orientation from velocity measurements. *IET Radar Sonar Nav*, 2(1):12-16. https://doi.org/10.1049/iet-rsn:20070025

Ehrman LM, Mahapatra PR, 2009. Impact of noncoherent pulse integration on RCS-assisted tracking. *IEEE Trans Aerosp Electron Syst*, 45(4):1573-1579. https://doi.org/10.1109/TAES.2009.5310319

Gokce M, Kuzuoglu M, 2015. Unscented Kalman filter-aided Gaussian sum filter. *IET Radar Sonar Nav*, 9(5):589-599. https://doi.org/10.1049/iet-rsn.2014.0088

Hong L, Wu S, Layne JR, 2004. Invariant-based probabilistic target tracking and identification with GMTI/HRR measurements. *IEE Proc Radar Sonar Nav*, 151(5):280-290. https://doi.org/10.1049/ip-rsn:20040858

Liu CY, Shui PL, Li S, 2011. Unscented extended Kalman filter for target tracking. *J Syst Eng Electron*, 22(2):188-192. https://doi.org/10.3969/j.issn.1004-4132.2011.02.002

Liu D, Zhao YB, Xu BQ, 2019. Tracking algorithms aided by the pose of target. *IEEE Access*, 7:9627-9633. https://doi.org/10.1109/ACCESS.2019.2890981

Menegaz HMT, Ishihara JY, Kussaba HTM, 2019. Unscented Kalman filters for Riemannian state-space systems. *IEEE Trans Autom Contr*, 64(4):1487-1502. https://doi.org/10.1109/TAC.2018.2846684

Mertens M, Ulmke M, Koch W, 2016. Ground target tracking with RCS estimation based on signal strength measurements. *IEEE Trans Aerosp Electron Syst*, 52(1):205-220. https://doi.org/10.1109/TAES.2015.140866

Musicki D, Song TL, 2013. Track initialization: prior target velocity and acceleration moments. *IEEE Trans Aerosp Electron Syst*, 49(1):665-670. https://doi.org/10.1109/TAES.2013.6404131

Rashedi M, Liu JF, Huang B, 2018. Triggered communication in distributed adaptive high-gain EKF. *IEEE Trans Ind Inform*, 14(1):58-68. https://doi.org/10.1109/TII.2017.2715340

Ruan Y, Hong L, 2006. Feature-aided tracking with GMTI and HRR measurements via mixture density estimation. *IEE Proc Contr Theory Appl*, 153(3):342-356. https://doi.org/10.1049/ip-cta:20045099

Skolnik M, 1962. Introduction to Radar System. Zuo QS, Xu GL, Ma L, et al., translators, 2010. Publishing House of Electronics Industry, Beijing, China (in Chinese).

Tang X, Tharmarasa R, McDonald M, et al., 2017. Multiple detection-aided low-observable track initialization using ML-PDA. *IEEE Trans Aerosp Electron Syst*, 53(2):722-735. https://doi.org/10.1109/TAES.2017.2664598

Tufts DW, Cann AJ, 1983. On Albersheim's detection equation. *IEEE Trans Aerosp Electron Syst*, AES-19(4):643-646. https://doi.org/10.1109/TAES.1983.309356

Villano M, 2014. SNR and noise variance estimation in polarimetric SAR data. *IEEE Geosci Remote Sens Lett*, 11(1):278-282. https://doi.org/10.1109/LGRS.2013.2255860

Xi YH, Zhang XD, Li ZW, et al., 2018. Double-ended travelling-wave fault location based on residual analysis using an adaptive EKF. *IET Signal Process*, 12(8):1000-1008. https://doi.org/10.1049/iet-spr.2017.0486

Zhang XY, Huang JL, Wang GH, et al., 2019. Hypersonic target tracking with high dynamic biases. *IEEE Trans Aerosp Electron Syst*, 55(1):506-510. https://doi.org/10.1109/TAES.2018.2884187

Zhang Y, Mu HL, Jiang YC, et al., 2019. Moving target tracking based on improved GMPHD filter in circular SAR system. *IEEE Geosci Remote Sens Lett*, 16(4):559-563. https://doi.org/10.1109/LGRS.2018.2878467

Zhou GJ, Pelletier M, Kirubarajan T, et al., 2014. Statically fused converted position and Doppler measurement Kalman filters. *IEEE Trans Aerosp Electron Syst*, 50(1):300-318. https://doi.org/10.1109/TAES.2013.120256